An exact analytical solution to the extended Navier-Stokes equations using the Lambert W function.*

Aditya Jaishankar[1] and Gareth H. McKinley†[1]

[1]Hatsopoulos Microfluids Laboratory, Department of Mechanical Engineering, Massachusetts Institute of Technology, Cambridge, MA, USA

Abstract

Micro channel gas flows are of importance in a range Micro Electro Mechanical Systems (MEMS). Due to the confined geometry of the channel, the mean free path of the gas can be comparable to the characteristic length of the micro channel, leading to slip-like flow behavior and strong diffusion-enhanced transport of mass and momentum. The Extended Navier Stokes Equations (ENSE) have successfully been used to model the slip behavior in rarefied gas flows as well as quantitatively predict the mass flow rate through the channel, without introducing any *ad hoc* parameters. The model involves accounting for self-diffusion due to local pressure gradients, and decomposing the total transport as the additive sum of individual convective and diffusive terms. In this paper, we show that it is possible to obtain exact analytical solutions to the ENSE equation set for the pressure and velocity field using the Lambert W function. We find that diffusive contributions to the total transport are only dominant for low average pressures and low pressure drops across the micro channel. For large inlet pressures, we show that the expressions involving the Lambert function predict steep gradients in the pressure and velocity localized near the channel exit. Using a limit analysis, we extract a characteristic length for this boundary layer. Our analytical results are validated by numerical calculations as well as experimental results available in the literature.

Keywords: Extended Navier-Stokes Equations, ENSE, Lambert W Function, Rarefied Gas Flow, Microchannel, MEMS, Knudsen

Introduction

Micro channel gas flows have elicited much research interest in recent years [1]. Such flows are frequently encountered in Micro Electro Mechanical Systems (MEMS) such as in thermal cooling systems for electronic devices [2], air damping of MEMS resonators [3; 4], gas chromatograph analyzers [5] and other applications. Theoretical understanding of macroscale fluid flows, where the continuum approximation holds, has existed for many decades and phenomena appearing at these

*Dedicated to Professor R. B. Bird on the occasion of his 90 birthday.

†Corresponding author: gareth@mit.edu

length scales are well understood and described in classic textbooks [6; 7]. Micro channel flows, however, exhibit many significant deviations from the predictions of the Classical Navier-Stokes Equations (CNSE) used to analyze macroscale flows. It has been known from the time of Maxwell [8] that the no-slip boundary condition can be violated in rarefied gas flows. Other deviations from classical macroscale flows include observations of higher mass flow rates through the channel [9] and nonlinear pressure drop along the channel [10].

These deviations from the classical results arise from rarefaction of the gas or the shrinking of the characteristic length scales of the flow geometry so that the mean free path λ of the gas becomes comparable to the characteristic length of the flow channel h [11]. Another important source of the deviation of micro scale flows from CNSE predictions is the relative importance of wall effects. The shrinking characteristic length scales of the channel lead to increasing surface to volume ratios, and hence the nature of interaction of the wall with the gas can strongly influence the flow properties. This is essentially a breakdown of the continuum approximation; to be able to neglect microscopic statistical fluctuations, we need a sampling volume with a characteristic length much bigger than the length scale h of the micro channel.

In a comprehensive overview of the first fifty years of Transport Phenomena [12], Bird highlights as some of the present day challenges "(e) What boundary and interfacial conditions in transport phenomena need to be clarified by use of molecular dynamics?" and "(h) What is the correct velocity boundary condition at the tube wall when a homogeneous mixture is flowing through the tube?"

We quantify the deviation from the continuum approximation with the help of the Knudsen number Kn defined as

$$\mathrm{Kn} = \frac{\lambda}{h} \tag{1}$$

where h is the characteristic length of the channel, and λ is the mean free path of the gas defined as [13]

$$\lambda = \frac{\mu}{P}\sqrt{\frac{\pi RT}{2}} \tag{2}$$

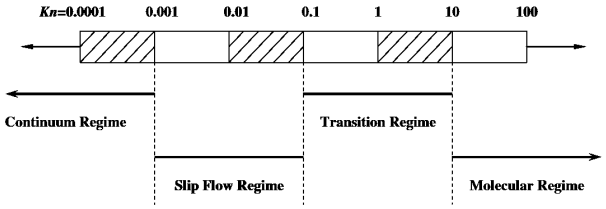

Figure 1: The different regime classifications of micro channel flows based on Knudsen number Kn. Figure is reproduced from [14].

Here μ is the viscosity of the gas, P is the pressure, R is the gas constant and T is the absolute temperature. In order of increasing Kn, the flow characteristics may be classified as a classical continuum flow, slip flow, transition flow or a free molecular flow [11]. Some typical values of Kn corresponding to these regimes are shown in Figure 1, which has been adapted from Dongari et al. [14]. Some of the earliest attempts to account for wall effects and to model the effects of slip in rarefied gas flows were due to Maxwell [8], who modeled the wall surfaces as being intermediate between perfectly reflecting and perfectly absorbing. Due to the roughness of the wall, a fraction σ of the gas molecules impacting it are absorbed by the wall, and subsequently re-emitted in a diffuse manner with a velocity distribution corresponding to a quiescent gas at that particular temperature. The remaining fraction $1 - \sigma$ is reflected specularly. With this assumption, Maxwell showed that the tangential slip velocity at the wall is given by

$$u_{\text{slip}} = \frac{2 - \sigma}{\sigma} \lambda \frac{\partial u}{\partial y} \tag{3}$$

where $\partial u / \partial y$ is the velocity gradient normal to the flow direction. For high Knudsen number flows, deviations from a first-order derivative model are observed, and hence higher order derivatives are frequently used to model slip in micro channel flows [11; 13; 15; 16]. Extensive reviews on the topic of slip in a micro channel are available [17].

It has been argued that using the CNSE together with the Maxwell slip velocity formulation is largely an empirical approach to modeling micro channel gas flows [18]. Furthermore, it does not account for local gradients in density which can create local fluxes due to self diffusion [19; 20]. A new approach has been proposed in a series of publications by Durst and co-workers (see for example [14; 20–22]). The underlying assumption in this theory is that the pressure gradient in the direction of the compressible flow provides an additional diffusive mode of mass transport, which

is accounted for analytically by adding an extra term to the CNSE. One therefore eliminates the need to include, in an *ad hoc* manner, the Maxwell slip velocity [14].

A treatment for the self diffusion of gases has been discussed in the landmark transport phenomena text by Hirschfelder, Curtiss and Bird. [23]. They note that in addition to familiar sources of momentum and mass diffusion that arise from concentration gradients in a multi-component system, there is another contribution to the diffusive flux that arises from the pressure gradient itself. The coefficients of self diffusion can be experimentally measured using, for example, the diffusion of one isotope of a gas into another, if the molecules are sufficiently heavy (see the discussion by Slattery and Bird [24]). These additional modes of transport are accounted for using a rigorous kinetic theory approach, making the mass flux expression significantly more complicated (see, for example, Pg. 516 of Hirschfelder et al. [23]). These additional contributions cannot be neglected when large pressure gradients exist in a rarefied gas flow field. The Extended Navier Stokes Equations (ENSE) proposed by Durst et al. [21] account for this mass and momentum transport due to self diffusion by replacing the velocity in the CNSE with a *total* velocity, that is a sum of convective and diffusive velocity terms.

The problem of pressure driven flow in of a compressible viscous gas through a tube is posed as a detailed exercise (2B.9) in R.B. Bird's second edition of *Transport Phenomena* [6]. Here it is suggested that there is additional contribution to the mass flux along the channel that arises from slip at the wall of the channel. It is suggested (based on empirical evidence) that the slip varies inversely with the pressure in the gas (consistent with equations (2) and (3)). The general form of the mass flux variation with pressure is sketched in a figure (Figure 2B.9 of reference [6]), and the insightful student might ask why the sketch shows not just an augmentation in the total flow rate through the channel but also a non-monotonic variation. To quantify and understand such observations it is necessary to have an analytic expression for the mass flux which describes the underlying transport phenomena.

In this paper, we provide for the first time exact analytical results obtained for micro channel gas flows modeled using the ENSE; currently only semi-analytical or numerical solutions are typically reported. Our presentation is intended to be didactic; we first provide a brief overview of the formulation of the model and the relevant equations. We then present the new analytical expression for the relationship between the total mass flux and the applied pressure difference, and discuss

the inherent non-monotonicities and non-linearities that arise. We also compare the results with experimental data to test their predictive ability. The utility of an analytic description of the flow field is demonstrated by using this new formulation to understand the boundary layer structure that can develop near the microchannel exit for sufficiently large inlet pressures. Finally, we use this detailed analytical understanding of this canonical fluid mechanics problem to construct a new flow state map for rarefied gas flows.

The Extended Navier Stokes Equations (ENSE)

At steady state and in the absence of any temperature gradients, the system of equations referred to for compactness as the ENSE for a single species are given by [25]

$$\frac{\partial(\rho u_i^T)}{\partial x_i} = 0 \tag{4}$$

$$\frac{\partial}{\partial x_i}\left(\rho u_i^T u_i^T\right) = -\frac{\partial P}{\partial x_j} - \frac{\partial}{\partial x_i}\left(\tau_{ij}^C - \frac{2}{3}\delta_{ij}\dot{m}_k^D u_k^C\right) \tag{5}$$

$$\tau_{ij}^C = -\mu\left(\frac{\partial u_i^C}{\partial x_j} + \frac{\partial u_j^C}{\partial x_i}\right) + \frac{2}{3}\mu\delta_{ij}\frac{\partial u_k^C}{\partial x_k} \tag{6}$$

along with the ideal gas equation of state

$$\rho = \frac{P}{RT} \tag{7}$$

It is assumed that the total mass transport in the extended model consists of a linear sum of convective and diffusive terms. The superscripts C, D and T in the above equations refer to convective, diffusive and total quantities respectively. The total velocity component in the i direction is given by $u_i^T = u_i^C + u_i^D$. The subscripts i, j, k refer to orthogonal coordinate directions and take the values 1,2 or 3. The other symbols in the above equations are the local density $\rho(\vec{x})$, the velocity $u(\vec{x})$, the local pressure $P(\vec{x})$, the local dynamic viscosity μ and the self diffusive mass flux in the k direction $\dot{m}_i^D = \rho u_i^D$. The Kronecker delta function is denoted by δ_{ij}. The self diffusive velocity in the i direction is given by the expression

$$u_i^D = -\frac{\mu}{\rho P}\frac{\partial P}{\partial x_i} \tag{8}$$

This diffusive velocity u^D is driven by gradients in the pressure and accounts for the Maxwellian slip-like velocity in a natural way, rather than introducing tunable parameters such as the parameter σ in equation (3).

In this paper we consider a rectangular micro channel of length L, width w and height h, with $h \ll w \ll L$. The lubrication approximation holds under these limits [7] and, assuming steady state flow, the ENSE simplify to [22]

$$\frac{\partial}{\partial x}\left(\rho u^T\right) = 0 \tag{9}$$

$$\frac{\partial^2 u^T}{\partial y^2} = \frac{1}{\mu}\frac{\partial P}{\partial x} \tag{10}$$

along with the boundary conditions

$$u^T\big|_{y=\pm h} = -\frac{\mu}{\rho P}\frac{\partial P}{\partial x} \tag{11}$$

where the walls of the micro channel are located at $y = \pm h$. These boundary conditions arise from the fact that the no-slip boundary condition applies to the convective velocity u^C at the wall surfaces ($u^C = 0$) so that only a diffusive flux is present locally.

Solving equation (10) for u^T and employing the boundary condition (11), Adachi et al. [22] show that

$$\dot{m}^T = \rho u^T = -\frac{\rho}{2\mu}(h^2 - y^2)\frac{dP}{dx} - \frac{\mu}{P}\frac{dP}{dx} \tag{12}$$

where $\dot{m}^T$ is the local mass flux per unit area and the total mass flow rate $\dot{M}^T$ through any cross section of the channel is given by

$$\dot{M}^T = w\int_{-h}^{h} \rho u^T \, dy \tag{13}$$

$$= -2hw\left(\frac{h^2 P}{3\mu RT} + \frac{\mu}{P}\right)\frac{dP}{dx} \tag{14}$$

We now proceed to find analytical expressions for the pressure field and the mass flow rate as well as the velocity field $u(x, y)$ in the channel. To the best of our knowledge, we present the first exact

analytical solutions to the ENSE for flow through a rectangular micro channel. Previous approaches have solved the integrated quantity in equation (14) numerically.

Results and Discussion

Consider the expression for the total mass flow rate $\dot{M}^T$ derived in equation (14). Because the mass flow rate remains constant through any arbitrary cross-section of the channel, we have $d\dot{M}^T/dx = 0$ and we can write this expression in the form

$$\left(\frac{h^2 P}{3\mu RT} + \frac{\mu}{P}\right)\frac{dP}{dx} = -C' \tag{15}$$

where $C' = \dot{M}^T/2hw$ is a constant of integration. This equation can be solved for P implicitly, and we determine C' from the boundary conditions at the inlet and outlet of the channel $P(0) = P_i$ and $P(L) = P_o$ to obtain

$$C' = \frac{1}{6RT}\frac{h^2}{L}\left(P_i^2 - P_o^2 + \frac{3\mu^2 RT}{h^2}\ln\frac{P_i^2}{P_o^2}\right) \tag{16}$$

We now non-dimensionalize equation (15) using $\bar{x} = x/L$ and $\bar{P} = P/P_c$ where L is the length of the micro channel and P_c is a characteristic pressure for an ideal gas given by $P_c = \mu\sqrt{3RT}/h$. As the pressure is increased to P_c, the mean free path given by equation (2) decreases to give a characteristic mean-free path λ_c or, equivalently, a characteristic Knudsen number given by $\mathrm{Kn}_c = \lambda_c/h = \sqrt{\pi/6}$ which characterizes the transition region in figure 1. Substituting these scalings into Equation (15) and (16) results in the simpler expression

$$\left(\bar{P} + \frac{1}{\bar{P}}\right)\frac{d\bar{P}}{d\bar{x}} = -\bar{C} \tag{17}$$

where $\bar{C} = (L/\mu)C'$. Solving this equation for the dimensionless pressure distribution along the channel $\bar{P}(\bar{x})$ with $\bar{P} = P_i/P_c = \bar{P}_i$ at $\bar{x} = 0$ and $\bar{P} = P_o/P_c = \bar{P}_o$ at $\bar{x} = 1$ we obtain the implicit expression

$$\bar{P}_i^2 - \bar{P}^2 + \ln\frac{\bar{P}_i^2}{\bar{P}^2} = \bar{P}_o^2\left(\mathcal{P}^2 - 1 + \frac{1}{\bar{P}_o^2}\ln\mathcal{P}\right)\bar{x} \tag{18}$$

where $\mathcal{P} = P_i/P_o = \bar{P}_i/\bar{P}_o$ is a characteristic pressure ratio for flow in the microchannel. At this point expression (18) can be evaluated using a suitable nonlinear equation solver or root finding algorithm; however additional insight can be gained by seeking an analytic expression for $\overline{P}(\bar{x})$. This equation admits itself to an exact closed form analytical solution given by

$$\frac{P(x/L)}{P_c} \equiv \bar{P}(\bar{x}) = \sqrt{W\left(\exp\left[-\overline{P}_o^2\left(\mathcal{P}^2 - 1 + \frac{1}{\overline{P}_o^2}\ln\mathcal{P}^2\right)\bar{x} + \bar{P}_i^2 + \ln\overline{P}_i^2\right]\right)} \tag{19}$$

where $W(x)$ is the Lambert W function defined to be the function $W(x)$ that satisfies the equation

$$W(x)\exp[W(x)] = x \tag{20}$$

Although it may not be widely known, the Lambert W function is ubiquitous in nature and appears in the solution of a number of mathematical as well as physical problems such as electrostatics, population growth, enzyme kinetics and quantum mechanics. It is similar to the trigonometric functions in the sense that it has no explicit closed form, but a very large number of physical problems are solved with relative ease by employing it in the solution [26]. Furthermore, almost all popular physical computing packages such as Mathematica, Matlab and Maple include full support for the Lambert W function, and utilize efficient algorithms to calculate its value at any point in its domain. Corless et al. [27] provide an excellent summary of the history and applications of $W(x)$.

We may now find explicit solutions for the total mass flow rate $\dot{M}^T$ and the velocity profile u^T by substituting equation (19) into equations (14) and (12) respectively to obtain

$$\dot{M}^T = \frac{\mu h\omega}{L}\left[\bar{P}_i^2 - \bar{P}_o^2 + \ln\left(\frac{\bar{P}_i}{\bar{P}_o}\right)^2\right] \tag{21}$$

$$u^T(\bar{x}) = \overline{P}_o^2\frac{h\sqrt{3RT}}{4L}\frac{\overline{P}(\bar{x})}{[1+\overline{P}^2(\bar{x})]}\left(\mathcal{P}^2 - 1 + \frac{1}{\overline{P}_o^2}\ln\mathcal{P}^2\right)\left(1 - \bar{y}^2 + \frac{2}{3\overline{P}^2(\bar{x})}\right) \tag{22}$$

where $\bar{y} = y/h$. We can also find the individual contributions to the total mass flux that arise from

the diffusive velocity field $u^D(\bar{x})$ and the convective velocity field $u^C(\bar{x},\bar{y})$ from equation (8):

$$u^D(\bar{x}) = \overline{P}_o^2 \frac{h\sqrt{3RT}}{6L}\left(\frac{\mathcal{P}^2 - 1 + (1/\overline{P}_o^2)\ln\mathcal{P}^2}{\overline{P}(\bar{x})(1+\overline{P}^2(\bar{x}))}\right) \tag{23}$$

$$u^C(\bar{x},\bar{y}) = \overline{P}_o^2 \frac{h\sqrt{3RT}}{4L}\left(\frac{\overline{P}(\bar{x})}{1+\overline{P}^2(\bar{x})}\right)\left(\mathcal{P}^2 - 1 + (1/\overline{P}_o^2)\ln\mathcal{P}^2\right)\left(1 - \bar{y}^2 - \frac{1}{3\overline{P}^2(\bar{x})}\right) \tag{24}$$

For a long narrow channel with $h \ll w$, the pressure gradient is unidirectional (along the channel) and the diffusive contribution does not vary across the channel. The total velocity field is in the micro channel is given by $u^T(\bar{x},\bar{y}) = u^C(\bar{x},\bar{y}) + u^D(\bar{x})$.

Equipped with these exact analytical solutions for the mass flow rate, the pressure field as well as the local velocity field, we next examine the behavior of these expressions under various conditions of inlet and outlet pressures and also compare the analytic expressions with experimental data. In figure 2, we show the scaled pressure $\Delta P_s = (\bar{P} - \bar{P}_o)/(\bar{P}_i - \bar{P}_o)$ calculated using equation (19) as a function of position along the channel $\bar{x}$. The curves correspond to different values of the inlet pressure $\bar{P}_i$ for a fixed (small) value of the outlet pressure $\overline{P}_o$. It is observed that the nature of the scaled pressure drop $\Delta\overline{P}_s$ strongly depends on the relative values of inlet and outlet pressures. We know that in the classical case the scaled pressure along the channel varies as $\Delta\overline{P}_s = 1 - \bar{x}$, and this linear result is independent of the inlet and outlet pressures $\bar{P}_i$ and $\bar{P}_o$. Accounting for diffusive terms makes the pressure drop highly nonlinear, and it is now a function of both $\bar{P}_i$ and $\bar{P}_o$. Moreover, for a fixed value of $\bar{x}$, say $\bar{x} = 0.5$, can be noted that the value of the scaled pressure varies non-monotonically at small values of $\bar{P}_i$ and saturates at high values of $\bar{P}_i$.

This non-linear evolution of the pressure profile predicted by the ENSE is more readily evident in the pressure *gradient* profiles. A closer examination of the curves in figure 2 shows the existence of an inflection point along the profile (i.e.) although the pressure gradient along the channel is always negative, its magnitude may vary non-monotonically. We can easily determine the pressure gradient along the channel by differentiating equation (19) with respect to $\bar{x}$ to obtain

$$\frac{d\overline{P}(\bar{x})}{d\bar{x}} = -\overline{P}_o^2 \frac{\overline{P}(\bar{x})}{2(1+\overline{P}^2(\bar{x}))}\left(\mathcal{P}^2 - 1 + (1/\overline{P}_o^2)\ln\mathcal{P}^2\right) \tag{25}$$

where we have used the fact that the derivative $W'(x)$ of the Lambert function given in equation (20)

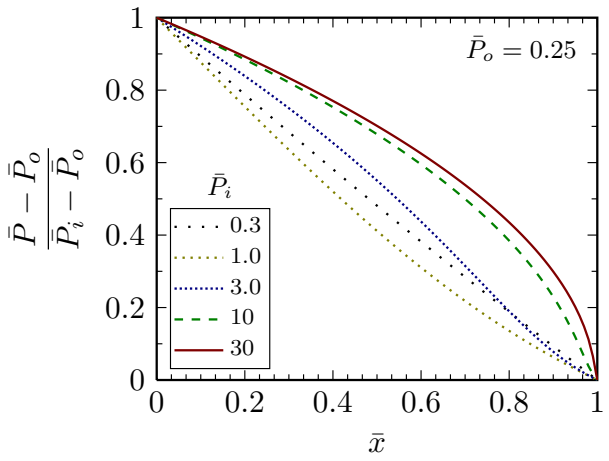

Figure 2: The non-dimensional pressure $\bar{P}(\bar{x}) = P/P_c$ as a function of non-dimensional position $\bar{x} = x/L$ along the micro channel analytically determined from equation (19). We observe that the pressure is a non-monotonic function of $\bar{P}_i$, and saturates for high inlet pressures $\bar{P}_i$. Furthermore, an inflection point is present in the curves, some of which are not readily apparent in the plots above on account of being very close to the exit.

is given by [27]

$$W'(x) = \frac{W(x)}{x(1+W(x))}; x \neq 0. \tag{26}$$

Plotting equation (25) in Figure 3 for different values of the dimensionaless inlet pressure $\bar{P}_i$, the non-monotonicity in the pressure gradient is readily apparent. In fact, we analytically find the location of this inflection point $\bar{x}^i$ using equation (25) by setting $d^2\overline{P}/d\bar{x}^2 = 0$ to be

$$\bar{x}^i = \frac{\bar{P}_i^2 + \ln \overline{P}_i^2 - 1}{\overline{P}_o^2(\mathcal{P}^2 - 1 + (1/\overline{P}_o^2)\ln \mathcal{P}^2)} \tag{27}$$

and the minimum (most negative) pressure gradient in the micro channel $d\overline{P}/d\bar{x}|_{\bar{x}=\bar{x}^i}$, which occurs at the inflection point, is given by

$$\overline{P}'_{\min} \equiv \frac{d\overline{P}}{d\bar{x}}\Big|_{\bar{x}=\bar{x}^i} = -\frac{1}{4}\left(\bar{P}_i^2 - \bar{P}_o^2 + \ln\left(\frac{\bar{P}_i}{\bar{P}_o}\right)^2\right) \tag{28}$$

where the prime denotes differentiation with respect to $\bar{x}$.

Deviations from the classical solution for the mass flow rate of a fluid through a micro channel is a fact that has been experimentally established [1; 10; 28–30]. The mass flow rate is observed to be higher than that predicted by the CNSE with the no-slip boundary condition. This occurs due

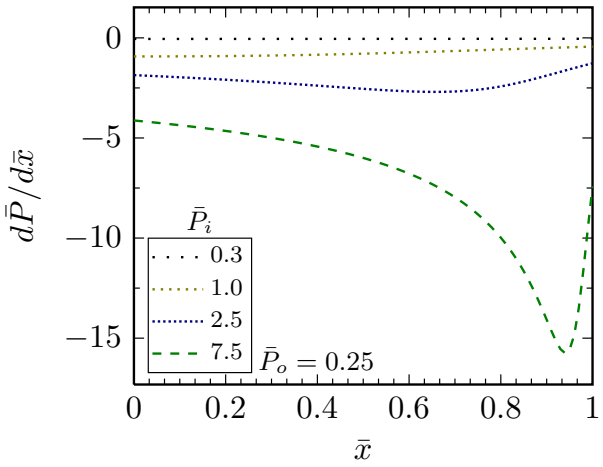

Figure 3: Analytically determined pressure gradient $d\overline{P}/d\bar{x}$ as a function of $\bar{x}$ (equation (25)) for a fixed value of the outlet pressure. There exists a point in the channel where the pressure gradient is most favorable (most negative), and the magnitude of the favorable pressure gradient increases with $\bar{P}_i$. The location $\bar{x}$ at which this occurs is also shifted towards $\bar{x} = 1$ as the pressure is increased (cf. equation (27)).

to the appearance of the additional 'slip-like' velocity contribution near the boundaries of the micro channel. This slip-like flow is modeled in the ENSE with the additional diffusive term without the need for introducing any fitting parameters or additional material constants, and hence this model should be able to predict the higher mass flow rate observed experimentally. Indeed, this is the case; in figure 4 we compare experimental measurements of the mass flow rate due to Maurer et al. [29] with the predictions of the ENSE presented in this paper (equation (21)). The values of channel dimensions and other experimental parameters used in this prediction are the same as those in the work of Maurer et al., and are summarized in the figure caption. We note that the the prediction is very good over a wide range of driving pressure differences, and the analytical solutions presented here captures the essential non-linearities and apparent slip phenomena observed in micro channel flows at moderate Knudsen number.

A useful way of representing the overall transport efficiency of the system is in terms of a conductance κ (i.e. the inverse of a flow channel resistance). For gas flow through a rectangular slit the ENSE predict that the conductance is thus given by

$$\kappa \equiv \frac{\dot{M}^T}{\Delta P} = \frac{\mu h w}{L P_c} \frac{1}{\bar{P}_i - \bar{P}_o} \left(\bar{P}_i^2 - \bar{P}_o^2 + \ln \frac{\bar{P}_i^2}{\bar{P}_o^2} \right) \tag{29}$$

The quantity $\overline{P}_i^2 - \overline{P}_o^2$ appears commonly in such problems (for example equation (29) and the abscissa of figure 4). Additional insight can be obtained if we rewrite this expression in terms

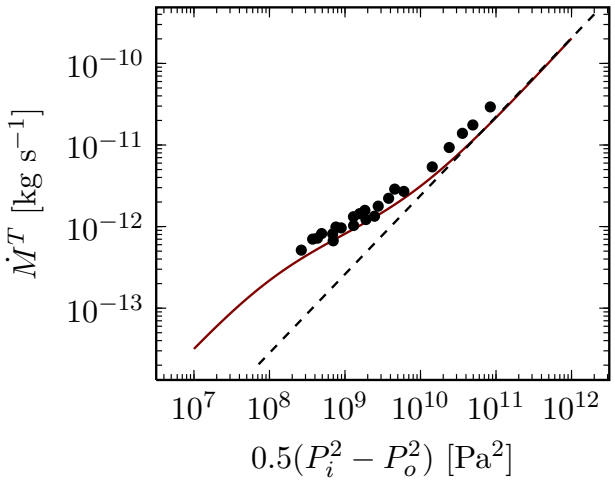

Figure 4: Prediction of the analytically derived solution to the ENSE compared to the experimental measurements taken directly from the values reported by Maurer et al. [29]. The agreement between the prediction and the data is good. The parameters used here are from Maurer at al. $\mu = 19.9 \times 10^{-6}$ Pa s, $h = 0.6$ μm, $w = 200$ μm, $L = 10$ cm, $T = 293$ K. The outlet pressure was held constant at $P_o = 12$ kPa. The black dashed line shows the CNSE solution for the mass flux.

of an average pressure $\langle P \rangle = (P_i + P_o)/2$ and a pressure difference $\Delta P = P_i - P_o$ such that $\overline{P}_i^2 - \overline{P}_o^2 = (\overline{P}_i + \overline{P}_o)(\overline{P}_i - \overline{P}_o) = \frac{1}{2}\frac{\langle P \rangle}{P_c} \cdot \frac{\Delta P}{P_c}$.

Using these identities we rewrite the conductance in terms of the average pressure $\langle P \rangle$ of the gas to obtain

$$\kappa = \frac{\mu h w}{L}\left(\frac{2\langle P \rangle}{P_c^2} + \frac{1}{\langle P \rangle - P_o}\ln\left(\frac{2\langle P \rangle - P_o}{P_o}\right)\right) \tag{30}$$

Furthermore, using equation (2), we can define a Knudsen number $\langle \mathrm{Kn} \rangle$ based on the average inlet pressure as

$$\langle \mathrm{Kn} \rangle = \sqrt{\frac{\pi}{24}}\frac{P_c}{\langle P \rangle} \tag{31}$$

In Figure 5a, we plot the conductance κ as a function of the average pressure $\langle \overline{P} \rangle$ in the micro channel. Whereas in the CNSE, the conductance monotonically increases with $\langle \overline{P} \rangle$ (because of the increasing density of the fluid), a distinct non-monotonicity is apparent in the case of ENSE: the conductance of the channel initially decreases with increasing average pressure and then increases to become indistinguishable from the classical limit. This non-monotonicity occurs due to the added diffusion transport mechanism. At low pressure differences, diffusive contributions of the flow resulting from the density gradient along the channel are vastly more efficient at transporting

mass and momentum through the micro channel compared to classical convective terms. It can be seen from figure 5(a) that the location of the minimum conductance (indicated by the symbols) is a function of the outlet pressure P_o.

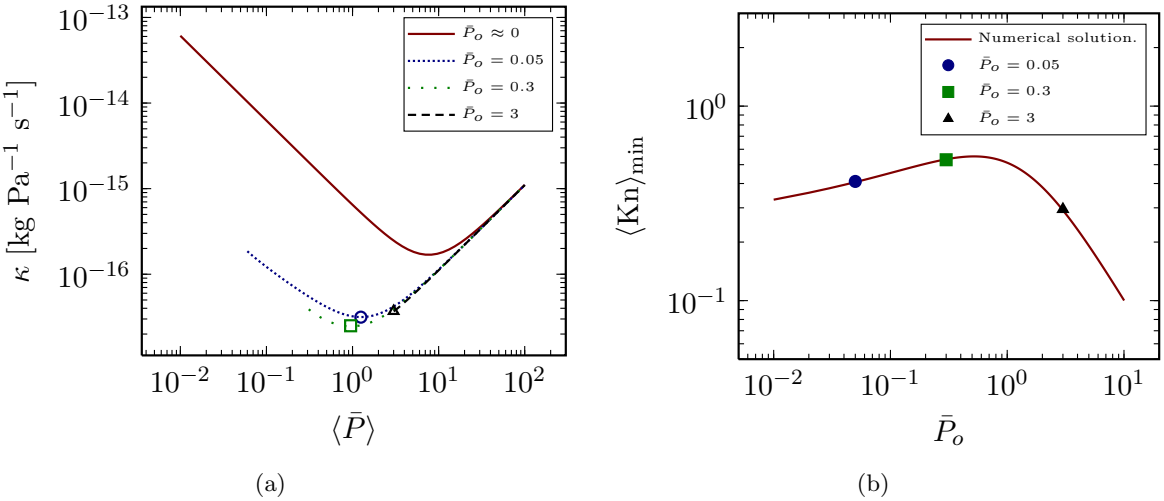

Figure 5: (a) The conductance κ of the micro channel as a function of the average pressure in the channel. In contrast to the prediction in the classical case in which the conductance increases linearly with average pressure, the CNSE predicts that the conductance varies non-monotonically with $\langle \bar{P} \rangle$. (b) The Knudsen number at minimum conductance calculated using the average pressure as a function of outlet pressure. The Knudsen number at minimum conductance varies non-monotonically.

In Figure 5b we plot the value of $\langle \mathrm{Kn} \rangle$ at that value of the outlet pressure for which κ is a minimum. Note that we are not able to find a simple analytical solution for the value of $\langle P \rangle$ at minimum conductance due to the non-linearity in equation (30). We therefore determine $\langle \mathrm{Kn} \rangle$ as a function of the dimensionless outlet pressure $\overline{P}_o$ numerically. Here we notice another non-monotonicity, and the Knudsen number $\langle \mathrm{Kn} \rangle_{\min}$ defined using the average pressure at which minimum conductance is obtained first increases with increasing outlet pressure and subsequently decreases as $\langle \mathrm{Kn} \rangle_{\min} \sim \overline{P}_o^{-1}$. For larger values of $\overline{P}_o$ (and hence larger $\langle \overline{P} \rangle$), the variation of conductance κ approaches the classical Navier-Stokes case, and κ varies monotonically with $\langle \overline{P} \rangle$. Hence the average pressure at minimum conductance equals $\overline{P}_i \approx \overline{P}_o$.

We can also compare the conductance defined by equation (29) with experimental measurements of the mass flux through a micro channel as a function of $P_i^2 - P_o^2$. In figure 6 we plot the experimental measurements of Maurer et al. with the analytic expression in equation (29). There are no adjustable parameters in this expression if the inlet and outlet pressures are specified in addition to the channel geometry. It is clear that the ENSE provide an excellent description in the

conductance of a rarefied gas through a micro channel, including the appearance of a minimum in the conductance at a specified value of the average pressure $\langle P \rangle = (1/2)(P_i + P_o)$ and the pressure driving force $\Delta P = P_i - P_o$. Also shown on this plot is the CNSE solution (black dashed line), in which $\langle \mathrm{Kn} \rangle$ increases linearly with $\overline{P}_o$.

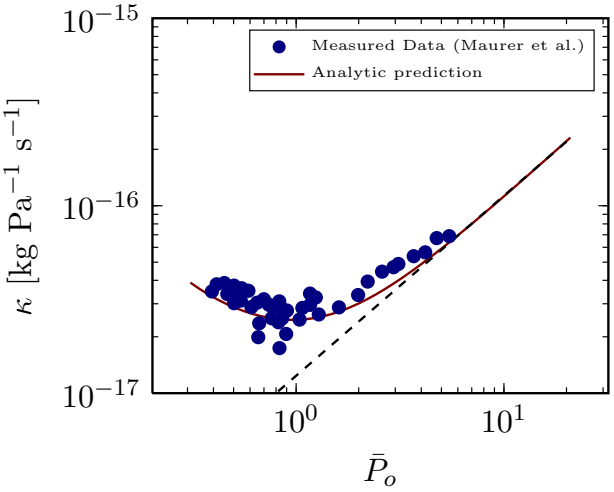

Figure 6: Comparison of the prediction of the analytical expression obtained in the present work for the conductance of a micro channel (equation (30)) against experimental data obtained by Maurer et al. [29]. The outlet pressure as well as fluid properties and micro channel geometry is the same as that in [29]. The prediction is very good and closely agrees with the experimental data. The black line shows the CNSE solution

We now turn to the velocity field $u^T(x, y)$ given by equation (22). In figure 7, we show the non-dimensional total velocity $\bar{u}^T(\bar{y}) = \frac{u^T}{\mu\sqrt{3RT}/4L}$ at different values of $\bar{x}$, for two different conditions: (a)$\bar{P}_i = 1$ and (b) $\bar{P}_i = 10$, keeping the outlet pressure fixed at $\bar{P}_o = 0.25$. We observe in Figure 7a that the velocity is non-zero at the channel walls, and this slip-like velocity arises from accounting for self-diffusion due to local gradients in pressure. In fact, for these values of $\bar{P}_i$ and $\bar{P}_o$, the diffusive velocity contribution (given by equation (23)) is a significant proportion of the total velocity.

This picture changes when the pressure ratio $\mathcal{P} = \bar{P}_i/\bar{P}_o$ is increased. In figure 7b, we show the same quantity $\bar{u}^T(\bar{y})$ with $\bar{P}_i = 10$ and $\bar{P}_o = 0.25$, corresponding to $\mathcal{P} = 40$. It is immediately observed that in this case, the convective terms in the velocity largely outweigh the diffusive terms. In this regime the slip-like velocity is relatively unimportant; this fact has been noted by other researchers, for example Adachi et al. [22]. The diffusive contribution to the mass flow rate is only important if it is of the same order of magnitude as the convective contribution. For this we require both of the independently variable pressures $\bar{P}$, $\bar{P}_i$ and $\bar{P}_o$ to be small. With increasing $\bar{P}_i$, the wall

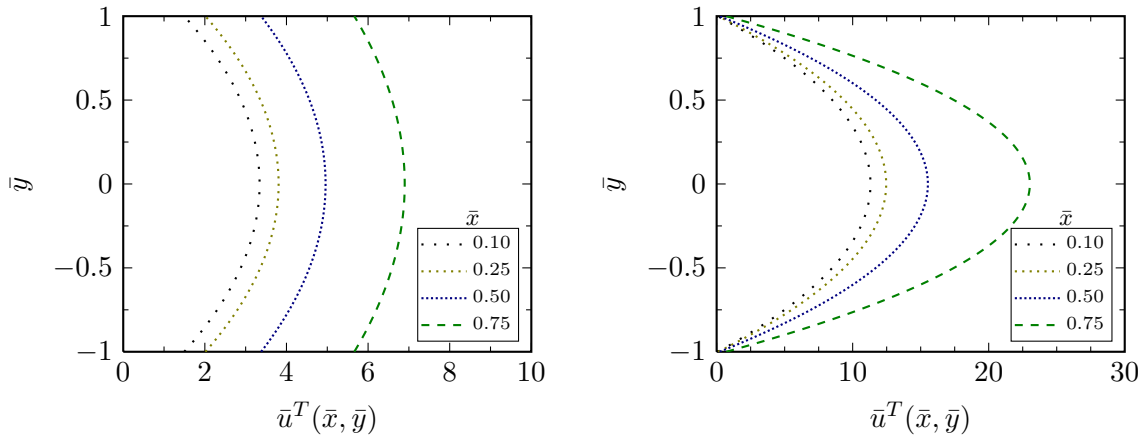

Figure 7: Velocity profiles in the micro channel at different locations $\bar{x}$. (a) $\bar{P}_i = 1$ and $\overline{P}_o = 0.25$ ($\mathcal{P} = 4$). The contribution of the diffusive velocity terms is a significant proportion of the total velocity and increases along the channel. (b) $\bar{P}_i = 10$ and $\overline{P}_o = 0.25$ ($\mathcal{P} = 40$). In this case, there is still slip at the walls, but its contribution to the total mass flux is negligibly small.

boundary condition begins to approach that of no-slip and the velocity profile becomes parabolic. This is reassuring because in the limit of high pressure, the Knudsen number is small (Kn $\ll 1$; cf. equation (2)), and microscale corrections should become relatively unimportant. However, we also note that because of the compressibility of the gas, there is still a steady increase in the local velocity down the channel in this case as shown in Figure 7(b). Moreover, the pressure profile along the micro channel is still highly non-linear and differs considerably from the CNSE solution, as can be seen from figure 2. As we show later, to approach the classical result $\Delta\overline{P} = 1 - \bar{x}$, we require both $\mathcal{P} \to 1$ and $P_i \gg P_c$.

To better visualize the evolution in the velocity field along the channel, we consider the quantity $\mathcal{U}(\bar{x}, \bar{y})$, which we call the scaled velocity, defined as

$$\mathcal{U}(\bar{x},\bar{y}) = \frac{u^T(\bar{x},\bar{y}) - u^T_{\min}}{u^T_{\max} - u^T_{\min}} \tag{32}$$

where $u^T_{\min}$ and $u^T_{\max}$ are the minimum and maximum velocities in the micro channel. It is clear from figures 7a and 7b that the minimum and maximum velocities lie somewhere along the $\bar{y} = \pm 1$ and $\bar{y} = 0$ lines respectively. This is also readily seen from equation (22). Moreover, if we isolate

the terms in equation (22) that depend on $\bar{x}$ and rewrite it as

$$u^T = \xi_1 \frac{\overline{P}(\bar{x})}{1+\overline{P}^2(\bar{x})}\left(\xi_2 + \frac{2}{3\overline{P}^2(\bar{x})}\right) \tag{33}$$

where $\xi_1 > 0$ and $\xi_2 \geq 0$ are coefficients independent of $\bar{x}$, and $\overline{P}(\bar{x})$ is given in terms of the Lambert W function. We can show that u^T is a strictly increasing function of $\bar{x}$ (because the pressure $\overline{P}(\bar{x})$ is a strictly decreasing function of $\bar{x}$.). Therefore, the minimum velocity in the channel is at $(\bar{x} = 0, \bar{y} = \pm 1)$ while the maximum in velocity occurs at $(\bar{x} = 1, \bar{y} = 0)$, which can now easily be found for any choice of $\bar{P}_i$ and $\bar{P}_o$.

Figures 8a-d show shaded plots of the scaled velocity $\mathcal{U}(\bar{x}, \bar{y})$ as a function of dimensionless channel coordinates. Each panel corresponds to a different value of $\bar{P}_i$ and the value of the outlet pressure was held to be constant at $\bar{P}_o = 0.25$. We observe that as the driving pressure difference is increased, the scaled velocity increases much more steeply in the vicinity of $\bar{x} \approx 1$. This behavior

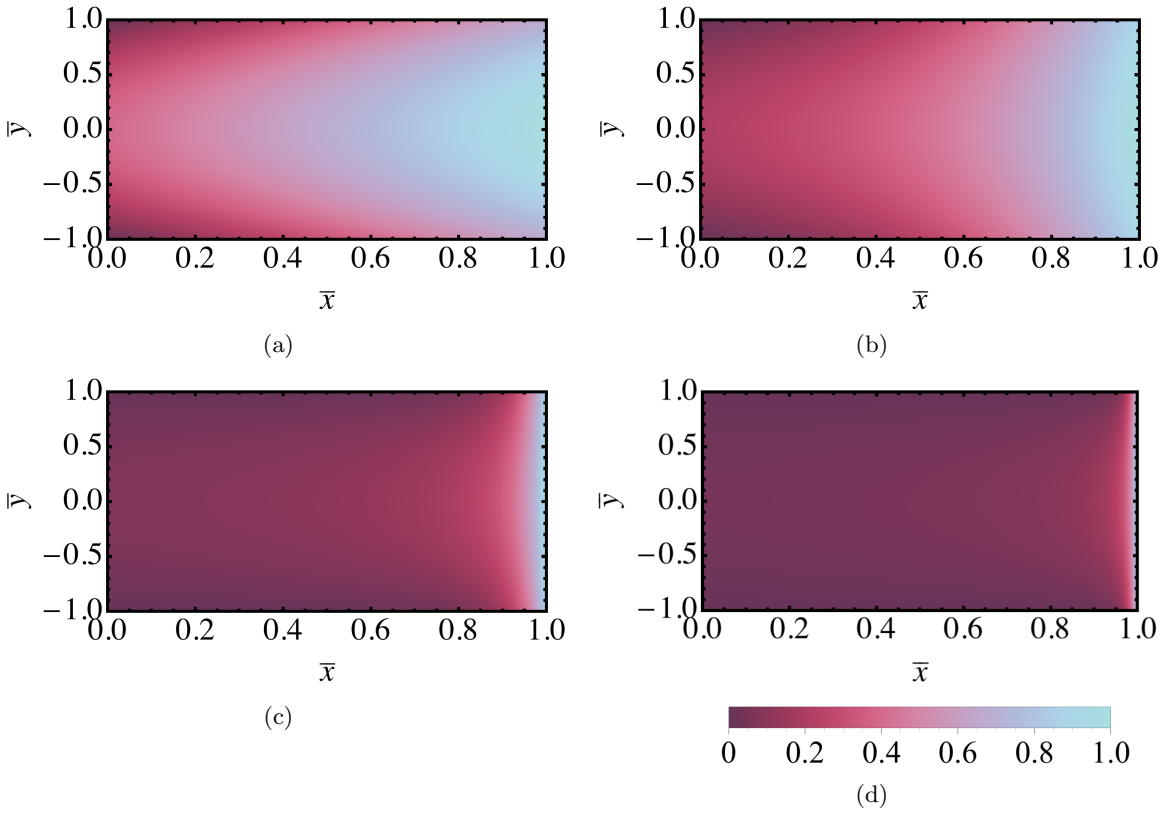

Figure 8: Magnitude of the scaled velocity $\mathcal{U}$ in the micro channel as a function of spatial position for different values of inlet pressure: (a) $\bar{P}_i = 0.3$, (a)$\bar{P}_i = 1.0$, (a)$\bar{P}_i = 5.0$, (a)$\bar{P}_i = 10$ at fixed outlet pressure $\overline{P}_o = 0.25$. For larger values of $\bar{P}_i$, the fluid undergoes a sudden increase in velocity in the vicinity of $\bar{x}$=1. Color scale bar shows values of $\mathcal{U}$ ranging from 0 to 1.

can be rationalized from the pressure gradient profiles presented in figure 3; as $\bar{P}_i$ is increased, the magnitude of the pressure gradient along the channel increases rapidly. In addition, equation (27) shows that in the limit of large pressure ratios $\mathcal{P} = \bar{P}_i/\bar{P}_o$, the location of the maximum favorable pressure gradient tends towards $\bar{x}^i \to 1$. This leads to the rapid increase of the gas velocity in the vicinity of $\bar{x} = 1$ for large $\mathcal{P}$. To better visualize this sudden change in the velocity near the outlet, in figure 9 we present line scans of the scaled centerline velocity $\mathcal{U}$ at different values of $\bar{P}_i$. The steep increase in the scaled velocity is clearly visible. This behavior stands in stark contrast to the classical incompressible solution, where the pressure gradient and the corresponding centerline velocity is constant throughout the channel.

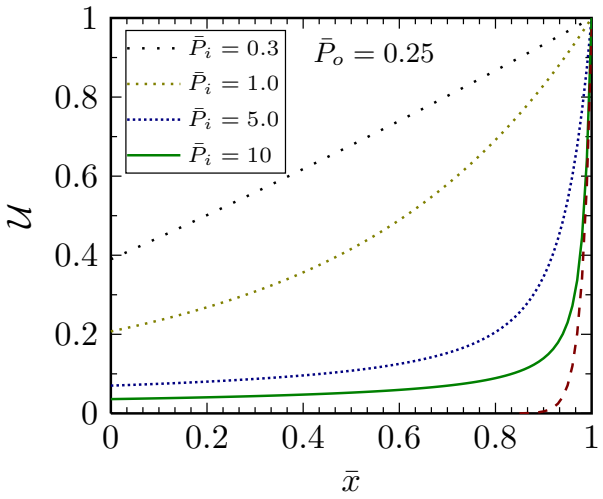

Figure 9: Scaled profiles of the centerline velocity along the micro channel for different values of $\bar{P}_i$. Increasing $\bar{P}_i$ leads to a steep increase in the scaled velocity close to $\bar{x} = 1$. The red dashed line shows the boundary layer approximation given in Table 1.

The rapid variation in the velocity field close to $\bar{x} \approx 1$ suggests a boundary layer analysis is appropriate when $\mathcal{P} \gg 1$. Through such an analysis we can extract a characteristic length scale for this boundary layer as well as the asymptotic behavior of pressure and velocity for different limits of $\bar{P}_i$ and $\bar{P}_o$.

We begin by a consideration of equation (18) which we reproduce here for clarity

$$\bar{P}_i^2 - \bar{P}(\bar{x})^2 + \ln \frac{\bar{P}_i^2}{\bar{P}^2(\bar{x})} = \bar{P}_o^2 \left(\mathcal{P}^2 - 1 + (1/\bar{P}_o^2) \ln \mathcal{P}^2\right) \bar{x} \tag{34}$$

Differentiating this equation with respect to $\bar{x}$ we obtain

$$\bar{P}(\bar{x}) + \frac{1}{\bar{P}(\bar{x})} = -\frac{\overline{P}_o^2}{2}\left(\mathcal{P}^2 - 1 + (1/\overline{P}_o^2)\ln \mathcal{P}^2\right) \tag{35}$$

We now perform the variable transformation $\xi = 1 - \bar{x}$ and let $\bar{P}(\bar{x}) = \overline{P}(1-\xi) = \overline{\psi}(\xi)$. Therefore equation (35) now becomes

$$\left(\overline{\psi} + \frac{1}{\overline{\psi}}\right)\frac{d\overline{\psi}}{d\xi} = \frac{\overline{P}_o^2}{2}\left(\mathcal{P}^2 - 1 + (1/\overline{P}_o^2)\ln \mathcal{P}^2\right) \tag{36}$$

Note that at $\bar{x} = 0$, $\xi = 1$ and $\overline{\psi}(1) = \overline{P}_o$. Similarly, $\overline{\psi}(0) = \overline{P}_i$. If desired a full matched asymptotic analysis of this equation can be carried out. Here we are primarily interested in the behavior of the pressure field in the vicinity of the exit of the channel ($\xi \ll 1$), (i.e) the inner expansion where $\psi(\xi) \approx \overline{P}_o$. We can consider two limits of this nonlinear equation: $\overline{P}_o \ll 1$ and $\overline{P}_o \gg 1$ depending on how large the outlet pressure at the end of micro channel is compared to the characteristic pressure scale $P_c = \mu\sqrt{3RT}/h$. In the former case, equation (36) simplifies to

$$\frac{1}{\overline{\psi}}\frac{d\overline{\psi}}{d\xi} \approxeq \frac{\overline{P}_o^2}{2}\left(\mathcal{P}^2 - 1 + (1/\overline{P}_o^2)\ln \mathcal{P}^2\right) \tag{37}$$

while for $\overline{P}_o \gg 1$ we obtain

$$\overline{\psi}\frac{d\overline{\psi}}{d\xi} \approxeq \frac{\overline{P}_o^2}{2}\left(\mathcal{P}^2 - 1 + (1/\overline{P}_o^2)\ln \mathcal{P}^2\right) \tag{38}$$

These differential equations can be easily solved to find the limiting behavior of the pressure field close to $\bar{x} = 1$. These results are presented in tables 1 and 2.

We can apply a similar approximation of the governing differential equation in the vicinity of the channel exit for the velocity field u^T. First we rewrite equation (12) in non-dimensional form and apply the same variable transformations described above to obtain

$$u^T = \frac{h\sqrt{3RT}}{2L}\left[1 + \frac{2}{3}\frac{1}{\overline{\psi}^2}\right]\frac{d\overline{\psi}}{d\xi} \tag{39}$$

	$\overline{P}_o \ll 1,\ \mathcal{P} \gg 1$	$\overline{P}_o \ll 1,\ \mathcal{P} \sim 1$
$\overline{P}(\bar{x})$	$\bar{P}_o \exp[(1/2)(\bar{P}_0^2\mathcal{P}^2 + \ln \mathcal{P}^2)(1-\bar{x})]$	$\overline{P}_o \exp[(1/2)(\mathcal{P}^2-1)(1-\bar{x})]$
$u^T(\bar{x})$	$\dfrac{h\sqrt{3RT}}{6L}\dfrac{\overline{P}_o^2\mathcal{P}^2 + \ln \mathcal{P}^2}{\overline{P}_o} \exp[-\frac{1}{2}(\bar{P}_0^2\mathcal{P}^2 + \ln \mathcal{P}^2)(1-\bar{x})]$	$\dfrac{h\sqrt{3RT}}{6L}\dfrac{\mathcal{P}^2-1}{\overline{P}_o} \exp[-\frac{1}{2}(\mathcal{P}^2-1)(1-\bar{x})]$

Table 1: Limiting expressions for pressure $\overline{P}(\bar{x})$ and velocity $u^T(\bar{x})$ for the case $\overline{P}_o \ll 1$.

	$\overline{P}_o \gg 1,\ \mathcal{P} \gg 1$	$\overline{P}_o \gg 1,\ \mathcal{P} \sim 1$
$\overline{P}(\bar{x})$	$\overline{P}_o\sqrt{\left(\mathcal{P}^2 + \dfrac{1}{\overline{P}_o^2}\ln \mathcal{P}^2\right)(1-\bar{x}) + 1}$	$\overline{P}_o\sqrt{(\mathcal{P}^2-1)(1-\bar{x}) + 1}$
$u^T(\bar{x})$	$\dfrac{h\sqrt{3RT}}{4L}\dfrac{\overline{P}_o\left(\mathcal{P}^2 + \dfrac{1}{\overline{P}_o^2}\ln \mathcal{P}^2\right)}{\sqrt{\left(\mathcal{P}^2 + \dfrac{1}{\overline{P}_o^2}\ln \mathcal{P}^2\right)(1-\bar{x}) + 1}}$	$\dfrac{h\sqrt{3RT}}{4L}\dfrac{\mathcal{P}^2-1}{\overline{P}_o\sqrt{(\mathcal{P}^2-1)(1-\bar{x}) + 1}}$

Table 2: Limiting expressions for pressure $\overline{P}(\bar{x})$ and velocity $u^T(\bar{x})$ for the case $\overline{P}_o \gg 1$. Although there is no exponential behavior in this case, when $\mathcal{P} \gg 1$, the functional dependence of the expressions for pressure and velocity are such that steep gradients occur near the channel exit.

which in the limits $\bar{P}_0 \ll 1$ and $\bar{P}_0 \gg 1$ simplify, respectively, to

$$u^T \cong \frac{h\sqrt{3RT}}{3L}\frac{1}{\overline{\psi}^2}\frac{d\overline{\psi}}{d\xi} \tag{40}$$

and

$$u^T \cong \frac{h\sqrt{3RT}}{2L}\frac{d\overline{\psi}}{d\xi} \tag{41}$$

We may now substitute into these equations the asymptotic form of the pressure from tables 1 and 2, according to the relevant magnitude of $\overline{P}_o$, to find the limiting expressions for the velocity field in the boundary layer near the exit. These results are also summarized in tables 1 and 2.

The exponential dependence of both $\overline{P}$ as well as u^T on $\bar{x}$ for low outlet pressures $\overline{P}_o \ll 1$ immediately suggests a characteristic length scale δ for the boundary layer region given by

$$\frac{\delta}{L} \sim \frac{1}{\overline{P}_o^2\mathcal{P}^2 + \ln \mathcal{P}^2} = \frac{3\mu^2 RT}{h^2 P_i^2 + 3\mu^2 RT \ln(P_i^2/P_o^2)} \tag{42}$$

For a fixed value of the outlet pressure $\overline{P}_o$, the boundary layer thickness decreases with increasing

$\overline{P}_i$ and this explains the form of the velocity profiles seen in figure 9. Equivalently, decreasing $\overline{P}_o$ also decreases the boundary layer thickness, although more slowly than increasing $\overline{P}_i$.

A different structure for the boundary layer at the exit is observed when the outlet pressure is high ($\overline{P}_o \gg 1$). The compressibility of the gas can still be important and there can still be a rapid decrease in the pressure near the exit. In this case, the pressure and velocity profiles have a square root and an inverse square root dependence on the distance from the exit, respectively. However the length scale of the boundary layer remains the same as that of Equation (42). The detailed expressions for this case are given in table 2.

Conclusion

In this paper we present, for the first time, exact analytical solutions to the Extended Navier-Stokes equations and obtain expressions for the pressure field, mass flow rate and velocity field for flow through a rectangular micro channel. The ENSE approach models the apparent slip-like flow of rarefied gases in micro channel geometries by accounting for mass transport due to local pressure gradients. Using the analytical expressions derived here, the nonlinear behavior of the pressure field and the resulting velocity field was examined in detail. The analytical expressions derived here are able to successfully capture the anomalous mass flow rate increases observed experimentally.

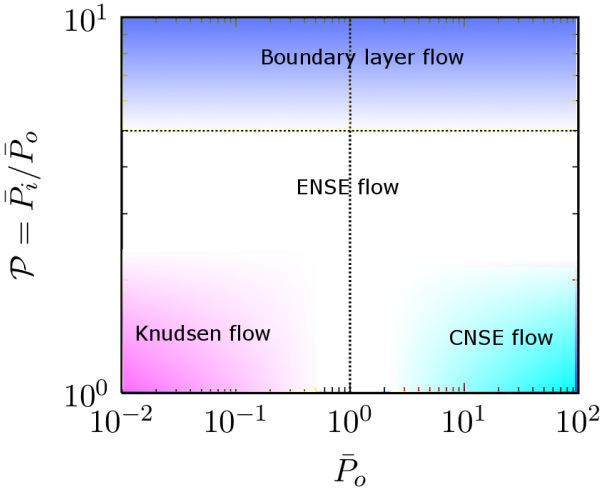

Figure 10: The different flow regimes for micro channel gas flows. Of note is the boundary layer flow regime, in which steep gradients in the pressure field as well as velocity field are localized in the vicinity of the channel exit.

The ability to obtain an analytic expression for the pressure profile $\overline{P}(\bar{x})$ along the channel (19)

in terms of the Lambert W function also helps us construct a more detailed version of the regime map that was shown schematically in Figure 1. This new two dimensional map is best represented in terms of the pressure ratio $\mathcal{P} = P_i/P_o = \overline{P}_i/\overline{P}_o$ that is driving the flow and either the average pressure $\langle P \rangle = (1/2)(P_i + P_o)$ in the channel or the scaled outlet pressure $\overline{P}_o = P_o/P_c$, each of which characterizes the thermodynamic state of the gas and the Knudsen number in the channel. We use the latter representation to construct Figure 10. The two dimensional velocity profile and the pressure profile along the channel are described by equations (19) and (22) for this entire space. For large outlet pressures ($P_o \gg P_c$) and small pressure drops ($\mathcal{P} \approx 1$), the ENSE for compressible viscous flow at moderate Knudsen numbers collapse to the classical Navier-Stokes equations. For low average pressures (corresponding to high Knudsen number) and small pressure differences, the flow approaches the Knudsen regime in which ballistic transport dominates. To describe this regime requires the solution of the Boltzmann equation using appropriate numerical techniques which depend on the Knudsen number range of interest [13].

As the pressure drop along the channel increases ($\mathcal{P} \gg 1$), the flow develops a boundary layer structure in which the largest velocity changes occur in a thin region of width δ near the channel exit. The specific form of the pressure profile or centerline velocity profile in this boundary layer regime depends on the magnitude of the outlet pressure P_o (compared to the characteristic value P_c). The results for both $P_o \gg P_c$ and $P_o \ll P_c$ are given in Tables 1 and 2 respectively. For extremely high pressure ratios, additional effects such as inertial acceleration and viscous heating may further modify the velocity field near the exit. The framework and methodology for dealing with such transport effects have been considered by Bird and colleagues in numerous publications (see for example [6; 12; 23]) but are beyond the scope of this work.

References

[1] C.-M. Ho and Y.-C. Tai, "Micro-Electro-Mechanical-Systems (MEMS) and Fluid Flows," *Annual Review of Fluid Mechanics*, vol. 30, pp. 579–612, Jan. 1998.

[2] Y. Joo, K. Dieu, and C.-J. Kim, "Fabrication of monolithic microchannels for IC chip cooling," *Proc. IEEE*, vol. 6, pp. 362–367, 1995.

[3] W. E. Newell, "Miniaturization of tuning forks.," *Science*, vol. 161, pp. 1320–1326, Sept. 1968.

[4] C. T. C. Nguyen, "Micromechanical resonators for oscillators and filters," in *Proceedings of the 1995 IEEE International Ultrasonics Symposium*, (Seattle, WA), pp. 489–499, 1995.

[5] S. C. Terry, J. H. Jerman, and J. B. Angell, "A Gas chromatographic air analyzer fabricated on a silicon wafer," *IEEE Transactions on Electron Devices*, vol. 26, pp. 1880–1886, 1979.

[6] R. B. Bird, W. E. Stewart, and E. N. Lightfoot, *Transport Phenomena*. New York: John Wiley & Sons, Inc., 1960.

[7] G. K. Batchelor, *An Introduction to Fluid Dynamics*. Cambridge University Press, 1967.

[8] J. C. Maxwell, "On stresses in rarified gases arising from inequalities of temperature," *Philosophical Transactions of the Royal Society*, vol. 170, pp. 231–256, 1879.

[9] J. C. Harley, Y. Huang, H. H. Bau, and J. N. Zemel, "Gas flow in micro-channels," *Journal of Fluid Mechanics*, vol. 284, pp. 257–274, Apr. 2006.

[10] J. Liu, Y.-C. Tai, and C.-M. Ho, "MEMS for pressure distribution studies of gaseous flows in microchannels," in *IEEE International Conference on Micro Electro Mechanical Systems.*, (Amsterdam, Netherlands), pp. 209–215, 1995.

[11] S. G. Kandlikar, S. Garimella, D. Li, S. Colin, and M. R. King, *Heat Transfer and Fluid Flow in Minichannels and Microchannels*. Oxford: Elsevier, 2006.

[12] R. B. Bird, "Five Decades of Transport Phenomena," *AIChE Journal*, vol. 50, no. 2, pp. 273–287, 2004.

[13] N. G. Hadjiconstantinou, "The limits of Navier-Stokes theory and kinetic extensions for describing small-scale gaseous hydrodynamics," *Physics of Fluids*, vol. 18, p. 111301, 2006.

[14] N. Dongari, A. Sharma, and F. Durst, "Pressure-driven diffusive gas flows in micro-channels: from the Knudsen to the continuum regimes," *Microfluidics and Nanofluidics*, vol. 6, pp. 679–692, Sept. 2009.

[15] N. G. Hadjiconstantinou, "Comment on Cercignanis second-order slip coefficient," *Physics of Fluids*, vol. 15, no. 8, p. 2352, 2003.

[16] S. K. Prabha and S. P. Sathian, "Calculation of thermo-physical properties of Poiseuille flow in a nano-channel," *International Journal of Heat and Mass Transfer*, vol. 58, no. 1-2, pp. 217–223, 2013.

[17] W. M. Zhang, G. Meng, and X. Wei, "A review on slip models for gas microflows," *Microfluidics and Nanofluidics*, vol. 13, no. 6, pp. 845–882, 2012.

[18] R. Sambasivam, "Extended Navier-Stokes Equations : Derivations and Applications to Fluid Flow Problems," *Ph.D Thesis, Universitat Erlangen-Nurnberg*, 2013.

[19] H. Brenner, "Navier-Stokes revisited," *Physica A: Statistical Mechanics and its Applications*, vol. 349, pp. 60–132, Apr. 2005.

[20] S. Chakraborty and F. Durst, "Derivations of extended Navier-Stokes equations from upscaled molecular transport considerations for compressible ideal gas flows: Towards extended constitutive forms," *Physics of Fluids*, vol. 19, no. 8, p. 088104, 2007.

[21] F. Durst, J. Gomes, and R. Sambasivam, "Thermofluiddynamics: Do we solve the right kind of equations," in *Proceeding of the international symposium on turbulence, heat and mass transfer*, (Dubrovnik), pp. 25–29, 2006.

[22] T. Adachi, R. Sambasivam, F. Durst, and D. Filimonov, "Analytical Treatments of Micro-channel and Micro-capillary Flows," in *3rd Micro and Nano Flows Conference*, (Thessaloniki, Greece), pp. 1–10, 2011.

[23] J. O. Hirschfelder, C. F. Curtiss, and R. B. Bird, *Molecular Theory of Gases and Liquids*. New York: John Wiley & Sons, Inc., 1954.

[24] J. C. Slattery and R. B. Bird, "Calculation of the Diffusion Coefficient of Dilute Gases and of the Self-Diffusion Coefficient of Dense Gases," *AIChE Journal*, vol. 4, no. 2, pp. 137–142, 1958.

[25] R. Sambasivam, S. Chakraborty, and F. Durst, "Numerical predictions of backward-facing step flows in microchannels using extended Navier-Stokes equations," *Microfluidics and Nanofluidics*, Sept. 2013.

[26] S. R. Valluri, D. J. Jeffrey, and R. M. Corless, "Some applications of the Lambert W function to physics," *Canadian Journal of Physics*, vol. 78, no. 9, pp. 823–831, 2000.

[27] R. M. Corless, G. H. Gonnet, D. E. G. Hare, D. J. Jeffrey, and D. E. Knuth, "On the Lambert W function," *Advances in Computational Mathematics*, vol. 5, pp. 329–359, 1996.

[28] J. Pfahler, J. Harley, H. Bau, and J. N. Zemel, "Gas and liquid flow in small channels.," *ASME Dynamic Systems and Controls Conference*, vol. 32, pp. 49–60, 1991.

[29] J. Maurer, P. Tabeling, P. Joseph, and H. Willaime, "Second-order slip laws in microchannels for helium and nitrogen," *Physics of Fluids*, vol. 15, no. 9, p. 2613, 2003.

[30] E. Arkilic, M. Schmidt, and K. Breuer, "Gaseous slip flow in long microchannels," *Journal of Microelectromechanical Systems*, vol. 6, pp. 167–178, June 1997.